Heavy-ion radiation test on LTC1668 DAC

A. Cotta Ramusino, S. Della Torre, L. Galli, A. Limonta, R. Malaguti, D. Nicolò, G. Signorelli, L. Silvestrin, F. Spinella, A. Tartari, M. Tessaro, J. Wyss and M. Zannoni

***Abstract*—We measured the heavy ion-induced single-event effect (SEE) susceptibility of the LTC1668 DAC from Linear Technology, to be used in the LiteBIRD JAXA space mission. LiteBIRD will be operated from the Lagrangian L2 in the early 30s, to map the microwave sky with three telescopes equipped with ∼4800 Transition Edge Sensors (TES) distributed onto three focal planes. The DAC we investigate here is a key item of the detector readout chain since it generates the MHz bias signal that is required by the TES Frequency-Division Multiplexing scheme. This 16-bit/50 Msps DAC has been identified as a critical element by its output spectral purity and low-power consumption (180 mW), which allow us to fulfil LiteBIRD's power budget constraints. Since this device doesn't exist in a space-qualified version, we have carried out a first characterization campaign at the heavy-ion facility Tandem-ALPI at INFN Legnaro National Laboratory (Italy) for a total irradiation time of ∼51 hours, to investigate its susceptibility to SEE. We have exposed the device to a beam of different ions with LET values ranging from 12 to 90 MeV cm^{-2}mg^{-1}. The device is moderately sensitive to SEE, with a threshold LET of 10.3 ± 1.3 MeV cm^2 mg^{-1} for SEU, 7.6 ± 2.0 MeV cm^2 mg^{-1} for SEL, and 9.2 ± 1.95 MeV cm^2 mg^{-1} for SET. This first campaign suggests that the use of DAC LTC1668 from space can be seriously considered.**

***Index Terms*—Space technology, CMOS integrated circuits, Radiation hardening (electronics), Single event latch-up, Ion radiation effects**

draft version: September 9, 2024
This work was supported by the financial support of INFN and the Italian Space Agency (ASI) through the LITEBIRD program, and the ASI Grants n. 2016[Pleaseinsert"PrerenderUnicode–˝intopreamble]24-H.1-2018 and 2020-9-HH.0.

A. Cotta Ramusino is with INFN Sez. di Ferrara, Ferrara, Italy (e-mail: cotta@fe.infn.it).

S. Della Torre is with CERN, Geneva, Switzerland and INFN, Sez. di Milano Bicocca, Milano, Italy (e-mail: stefano.della.torre@cern.ch).

L. Galli is with INFN, Sez. di Pisa, Pisa, Italy (e-mail: luca.galli@pi.infn.it).

A. Limonta is with Dipartimento di Fisica dell'Università di Milano Bicocca and INFN, Sez. di Milano Bicocca, Milano, Italy (e-mail: andrea.limonta@unimib.it).

R. Malaguti is with INFN Sez. di Ferrara, Ferrara, Italy (e-mail: malaguti@fe.infn.it).

D. Nicolò is with Dipartimento di Fisica dell'Università di Pisa and INFN, Sez. di Pisa, Pisa, Italy (e-mail: donato.nicolo@pi.infn.it).

G. Signorelli is with INFN, Sez. di Pisa, Pisa, Italy (e-mail: giovanni.signorelli@pi.infn.it).

L. Silvestrin is with Dipartimento di Fisica dell'Università di Padova and INFN, Sez. di Padova, Padova, Italy (e-mail: luca.silvestrin@unipd.it).

F. Spinella is with INFN, Sez. di Pisa, Pisa, Italy (e-mail: franco.spinella@pi.infn.it).

A. Tartari is with Dipartimento di Fisica dell'Università di Pisa and INFN, Sez. di Pisa, Pisa, Italy (e-mail: andrea.tartari@pi.infn.it).

M. Tessaro is with Dipartimento di Fisica dell'Università di Padova and INFN, Sez. di Padova, Padova, Italy (e-mail: mario.tessaro@pd.infn.it).

J. Wyss is with INFN, Sez. di Padova, Padova, Italy (e-mail: wyss@unicas.it).

M. Zannoni is with Dipartimento di Fisica dell'Università di Milano Bicocca and INFN, Sez. di Milano Bicocca, Milano, Italy (e-mail: mario.zannoni@unimib.it).

I. Introduction

LiteBIRD is a next-generation space mission for primordial cosmology and fundamental physics [1]. The mission's goal is to detect the signal of the primordial gravitational waves in the so-called B-mode polarization of the cosmic microwave background — a faint signal that resides in the largest angular scales [2]. If discovered, it would solve several cosmological questions going beyond the current limits in understanding the Universe's evolution. Given the foundational importance of this goal, this signal is targeted by many past and future ground-based CMB experiments (see e.g., [3]), while LiteBIRD will be the first satellite after Planck [4]. The space constitutes an ideal environment because it provides access to the largest angular scales (where the inflationary signal is the highest) and to the high-frequency range (which, on the ground, is limited by the Earth's atmosphere). LiteBIRD is an international multi-partner project, selected by JAXA in 2019 as a strategic large-class mission with an expected launch in the early Thirties. The mission duration length is 36 months, during which it is expected to achieve an unprecedented total sensitivity of 2.2 $\mu K \cdot arcmin$. The satellite will operate on a Lissajous orbit around the Sun-Earth L2 point to avoid the influence of radiation from the Sun, Moon, or Earth. The 4'732 superconducting TES (transition-edge sensors) detectors of LiteBIRD are read out in parallel using a frequency-division multiplexing technique where one bias signal is sent to several detectors on almost 60 different carriers and amplified by a SQUID[1]. For the design of the warm readout, the AD768 DAC was originally considered to generate the carrier and null signals. It was selected due to its low $1/f$ noise and its availability as a space-qualified component. However, this DAC is power-hungry and accounts for a non-negligible part of the readout electronics power budget. An alternative DAC, the LTC1668 (described in Tab. I), offers the same performance with at least half of the power consumption, but this component need to be space qualified.

While operating in space, the electronics of the satellite will face the harsh space radiation environment that is permeated by energetic high-energy ionized particles. These particles can directly penetrate the shielding of most spacecraft, and even create ionizing secondaries via nuclear interactions with the material of the satellite. These Cosmic Rays (CR) thus represent a potential radiation hazard for the electronics of the detectors (see, e.g., [5]–[7]). The effects of CR may be organized into three categories [8]: Total Ionizing Dose (TID) effects, Displacement Damage Dose (DDD) effects, and Single

[1]i.e., Superconducting Quantum Interference Device; it is a very sensitive magnetometer used to measure extremely tiny magnetic fields and used as an ultra-sensitive ammeter.

2024 RADECS Data Workshop | 979-8-3315-3631-2/24/$31.00 ©2024 IEEE | DOI: 10.1109/RADECS61975.2024.11017543

Event Effects (SEE). TID and DDD effects bring gradual global degradations of device parameters; on the other hand, SEE are stochastic effects due to the interactions of single particles; they are localized effects and can lead to a seemingly spontaneous transient within a region of the circuit [9]. SEE appear as random glitches in electronic systems that may cause both unwanted system responses (e.g., bit flips) or catastrophic (at worst) system failures [9]. SEE may be either destructive (or potentially destructive) effects or transient effects [8].

In this work, we explore the transient effect of SEE due to heavy-ions interaction with the LTC1668 DAC BiCMOS active layers. This component was already tested up to 70 krad with photons at γELBE irradiation facilities where no TID effects are observed on linearity, noise, and degradation, allowing LTC1668 to be a suitable COTS electronics component for space use.

TABLE I
DESCRIPTION OF LTC1668

Part description:	LTC1668IG 16–bit, 50Msps DAC
Manufacturer:	Linear Technology
Package:	28–pin SSOP
Technology:	BiCMOS
Samples used:	Tested 4 samples out of a package of 10
Die area:	2 mm $\times$ 2.95 mm = 5.9 mm^2

II. RADIATION HARDNESS SETUP

Using heavy ions from the XTU Tandem at INFN-LNL, the Italian National Laboratories of Legnaro, we tested four samples (hereafter called DUT – Device Under Test – and referred to in this text as DUT0, DUT1, DUT2, and DUT3) to assess three kinds of SEE: Single Event Upset (SEU), Single Event Latch-up (SEL) and Single Event Transient (SET). SEU occurs when the energy transient influences a node that is storing information, causing a corrupted state that may be either unrecognizable, unreadable, or unstable. This upset can, in turn, lead to a circuit error if this corrupted state alters legitimate information stored in or propagating through the circuit. This kind of event belongs to a class of errors that are static but can be corrected by a rewrite, power cycle corrects, or resets the part to proper operation with no permanent damage [9]. Single event latch-up (SEL) is a potentially destructive triggering of a real or parasitic pnpn thyristor structure in the device [8]; when this event occurs, a regenerative current passes through the device: if the current levels are benign, the causer error can be reset and the functionality restored, while if the regenerative current energy exceeds the thermal dissipation of the affected region, these effects can cause melting and permanent physical damage to the circuit [9]. Finally, SET is an upset in analog electronics (i.e., a current transient) which can be interpreted as a false signal; generally the seriousness of the SET depends on where in the linear circuit the ion strikes, on the settings of the circuit, on the filtering of the signal and on how the signal is used [8].

TABLE II
USED TANDEM ION BEAMS ALONG WITH CORRESPONDING ENERGY, RANGE IN SI AND SRIM CALCULATED SURFACE LET VALUE FOR NORMAL INCIDENCE OF THE IONS AS THEY ENTER SILICON.

Ion	Energy [MeV]	Range in Si [μm]	LET in Si [MeV cm^2/mg]
^{35}Cl	160^a, 171^b	46, 49.71	13.05, 12.68
^{58}Ni	220	37.03	29.36
^{79}Br	228	31.2	41.96
^{107}Ag	266	29.03	58.39
^{127}I	249^a, 276^b	27.74, 29.53	63.66, 65.37

^{a}Energy value of the beam during the 2022 campaign
^{b}Energy value of the beam during the 2021 campaign

A. The irradiation beam

The irradiation test was performed at the SIRAD irradiation facility [10] in February 2021 and June 2022 for a total irradiation time of $\sim$51 hours. Among the cocktail of ions available, we chose five ions (i.e. Cl-35, Ni-58, Br-70, Ag-107, and I-127) with LET values in Silicon ranging from 12.68 MeV cm^2/mg up to 65.37 MeV cm^2/mg (see Tab. II). The effective LET, see Eq. (1), is then increased by rotating the device under test through several angles [8].

$$LET_{eff}(\theta) = LET_0 \times \cos^{-1}(\theta) \quad (1)$$

where LET_0 is the value for normal incidence (θ = 0).

The protective lid on top of the device was chemically removed to expose directly the active area to the ion beams. The LET_0 values in Table II are calculated at the surface of silicon. A more accurate SRIM calculation of the LET should consider the presence of a thin layer of oxide and metal materials, as well as the loss of energy inside the active volume. If thick enough, this loss would invalidate the assumption of a constant linear energy deposition. In our case, the width of the passive layers on top of the active layer is not known, but we were able to measure the active volume to be $\sim 1\mu m$ thick. In the overall trend of SEE measurements, as a function of ion species and angle of inclination, we do not find any evidence of effects due to dead layers for the heaviest ions with the shortest range. Thus, the surface LET value of the ions as they enter silicon is considered a good estimator.

The irradiation was performed in a vacuum chamber equipped with a movable and tiltable stage that allows the alignment of the DUT with the ion beam. The position and tilt of the DUT are monitored with a CCD camera looking inside the vacuum through a set of mirrors. A laser beam is used to align the various DUTs with the beam, while dedicated software allows to record the encoder data to re-position all DUTs correctly after the vacuum chamber has been closed. Vacuum feed-through (high-density and coaxial) is available to carry the signals in/out of the chamber.

The DUT region is surrounded by four PIN-diodes that count the number of impinging ions during irradiation to estimate the received flux. A second set of four PIN-diodes can be placed instead of the DUT at any time to cross-check the total flux. The beam homogeneity (better than 10%) over the active area is guaranteed by defocusing the beam.

A flux of $10^3 \sim 10^5$ ions/cm^2/sec is available. A beam blocker guarantees the correct timing of the irradiation of the DUTs. The real-time ion flux and the total fluence are recorded by the system and stored together with the accelerator parameters. Irradiation of the devices was divided in *runs* of ∼20 minutes, including dead time during SEE detection. Each DUT received, at the end of the campaign, a minimum irradiation fluence of $\sim 7.5 \times 10^5$ cm^{-2} from at least two different ions covering a LET range from 12 to 90 MeV cm^2 mg^{-1} (see Tab. III).

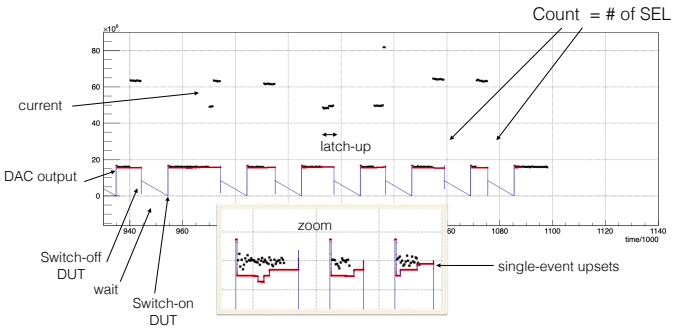

Fig. 1. Typical sequence of data acquisition during one test run.

B. The experimental set-up

The readout system of the test is based on an ArriaV GX FPGA (GEMROC board, developed in the framework of the BESIII experiment) which runs at 166 MHz, coupled to custom transition boards to interface the current output of the LTC1668 to the input ADCs. The system implements the high-resolution readout of 3 independent current/voltages at 24 bits at 26kHz and a lower resolution readout of device currents and temperatures. This high-resolution, slow ADC, is used to detect SEL and SEU. The transition boards send a copy of each of the four DAC outputs to a digital scope readout at 50 MHz to detect transients (i.e., SET). The 16-bit digital scope features a sampling rate of 62.5 MS/s, with a maximum temporal resolution of 16 ns/bin. The system allowed us to be sensitive to 15 bits out of 16 with the high resolution, low-speed ADC, while 10 bits out of 16 with the low resolution, high-speed one.

The LTC1668 has been tested with a ±5V power supply. During irradiation the contents of the irradiation registers were frozen, i.e., the input of the DAC was held constant, the clock signal was stopped, and the output was digitized at 24 bits with a 16kHz rate. The DAC pattern was alternatively programmed with the content 0xA5A5 or 0x5A5A, for which the output of the DAC was set at the mid-range of the high-resolution ADC. We note that the RMS of the 24-bit ADC readout was ≈100 ADC counts, while the total span of the DAC as recorded by the ADC was ≈ 0x61A800, corresponding to 23 bits. We conclude, then, that we were effectively sensitive to 15 out of 16 bits of the DAC. The DUTs were tested at room temperature, i.e., the temperature they reached in the vacuum when switched on. This turned out to be in the range of 28° to 35 °C. LiteBIRD electronics, once on orbit, would operate

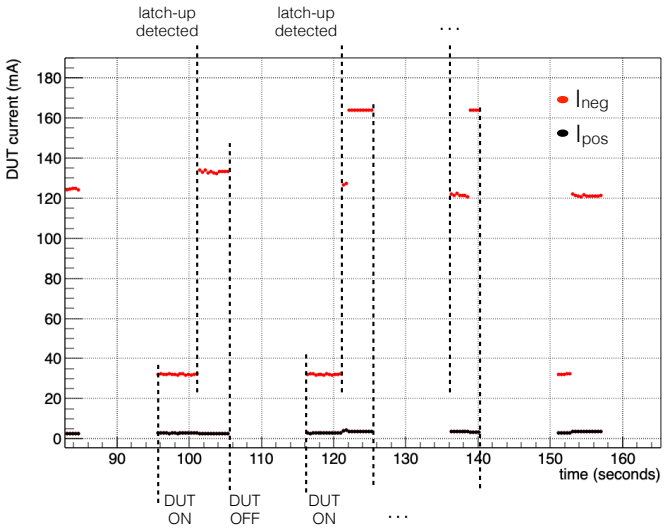

Fig. 2. Typical behaviour of positive and negative current of LTC1668 during irradiation.

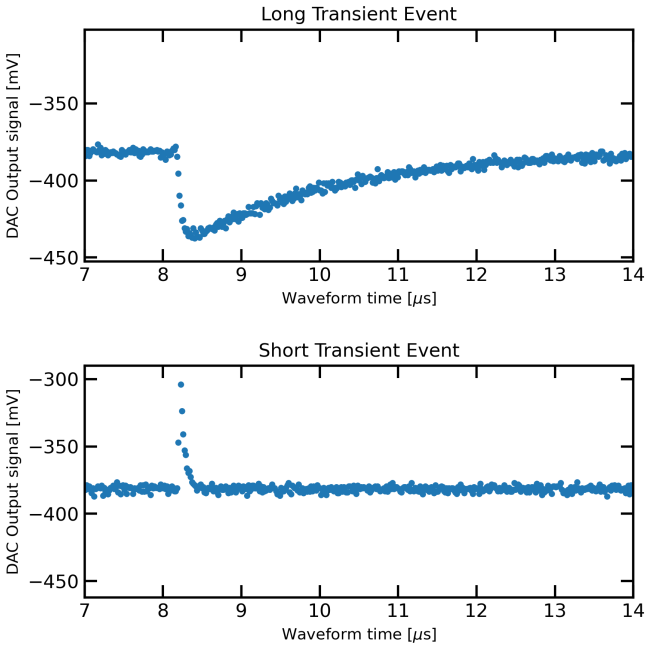

Fig. 3. Examples of transient events recorded during the test with the 16-bit Picoscope.

in a thermalized environment with an expected range from ∼10° to ∼30 °C, and thus the actual test should represent the worst-case operation condition. Future tests will assess the operability in more extreme conditions.

We monitored positive and negative current, reference voltage and DUT temperature. Changes in DAC output are attributed to upsets or transients. Upsets are defined as a definite change of output, while transients as glitches in the output. We identified SEUs using the high-resolution, low-speed DAC, while SELs with the lower resolution, high-speed ADC. A typical sequence of data acquisition with both SELs and SEUs visible is presented in Fig. 1.

C. SEE Identification

The latch-up (SEL event) was identified by monitoring the positive and negative current drawn by the DUT. During normal operation, the DUT draws I_{pos} = 32 mA and I_{neg} = 2.7 mA. A sudden current or temperature increase was attributed to a latch-up. We set as SEL trigger threshold $\pm$40 mA in current and 50°C in temperature. At this point, the current was monitored and recorded for a few seconds (i.e. $\sim$4s), after which the DUT was switched off, waited for 3 to 20 seconds according to the test conditions, and switched on again. The typical behaviour of the DUT current is shown in Fig. 2.

The data stream of the high-resolution ADC is written to a file, which is analysed offline to recognize Heavy-ion Event Upsets. We applied a procedure that compares two moving windows of 64 data points, if the difference of the two computed ADC counts is greater than a threshold of 180 we count it as a SEU. We estimated that using this threshold we were able to distinguish upset events for 15 most significant bits, out of the 16 bits device resolution, with respect to the noise in the acquisition system.

SET was recorded during each run using a digital-scope (Picoscope™ 5000 Series) based high-speed DAQ system. One copy of the DAC output was sent to a 16-bit digital scope that triggered when the DAC signal exceeded a window of $\pm 5\sigma$. Since the average output level can change following SEUs, the average level is continuously monitored by a moving-average algorithm calculated using the first 512 pre-trigger samples, corresponding to 8.192μs, which are used to compute also the RMS signal. With these settings, we could detect both positive and negative excursions, but we were sensitive also to SEUs, SELs, and spurious events. Data were re-processed offline to eliminate spurious triggers and to classify different types of transients. We found that, during the acquisition time, a high number of short transient events were triggered. These events are probably due to the tails of the noise distribution, which increase in the harsh environment of the experimental cavity. Since we are interested in long transients only, during the offline analysis we reject all events shorter than 80 ns (corresponding to 5 samples). Examples of SET events measured during the test are reported in Figure 3.

III. Test results

Including the two test periods, we performed $\sim$ 100 runs, including calibration and testing. The test log of the run good for analysis is reported in Tables V,VI, and VII. The Total Ionizing Dose received during the test is reported in Tab. III. The estimation was performed using the *TID Fluence converter calculator* developed by the ASIF/SR-Niel framework [11]. The deposited TID in rad is calculated using the equation (section 3.1.4 in Ref. [12]):

$$TID = F \times LET \times 1.6 \times 10^{-5}. \quad (2)$$

where F is the ion Fluence in the plane normal to the beam measured in particles/cm^2 and LET is expressed in MeV cm^2 mg^{-1}. The evaluation of the LET used in the formula was obtained from SRIM[2] and we assume that the energy lost by the incoming particle is fully absorbed by the medium – for instance, the medium is supposed to be thick enough to fully absorb the kinetic energy of emitted delta rays – and the particle energy is almost constant while traversing the absorber.

TABLE III
Total exposed fluence for each DUT along with the ionizing dose absorbed

DUT	Ions	Energy [MeV]	Total Fluence [cm^{-2}]	Ionizing Dose [rad]
DUT0	Cl-35	171	6.09E+07	1.46E+04
DUT0	Ni-58	220	5.29E+07	2.74E+04
DUT0	Ag-107	266	4.96E+06	4.76E+03
DUT0	I-127	276	7.49E+05	7.84E+02
	TOTAL		**1.19E+08**	**4.68E+04**
DUT1	Cl-35	160	5.91E+07	1.37E+04
DUT1	Cl-35	171	6.02E+07	1.44E+04
DUT1	Ni-58	220	2.44E+07	1.38E+04
DUT1	Br-79	228	3.19E+06	2.30E+03
DUT1	Ag-107	266	1.17E+07	1.24E+04
DUT1	I-127	249	1.19E+07	1.27E+04
DUT1	I-127	276	4.60E+05	4.81E+02
	TOTAL		**1.70E+08**	**6.94E+04**
DUT2	Cl-35	160	3.84E+06	9.34E+03
DUT2	Cl-35	171	4.80E+07	1.22E+04
DUT2	Br-79	228	6.69E+05	5.19E+02
DUT2	Ag-107	266	8.14E+06	8.79E+03
DUT2	I-127	249	4.23E+06	5.04E+03
	TOTAL		**9.94E+07**	**3.58E+04**
DUT3	Cl-35	160	4.53E+07	1.15E+04
DUT3	Br-79	228	9.13E+05	7.31E+02
DUT3	I-127	249	3.00E+06	3.64E+03
	TOTAL		**4.92E+07**	**1.59E+04**

A. SEE cross-section

The cross-section was computed normalizing to the acquisition lifetime and considering the effective flux in the tilted situation. The measured cross-section was fitted using the Weibull function:

$$\sigma(L) = \sigma_f \left[1 - \exp\left(-\frac{L - L_{th}}{W}\right)^S\right] \quad (3)$$

L_{th} is the threshold value for producing the single event effect, σ_f is the final (saturation) cross-section value for high LET, while the width and shape parameters W and S describe the transition smoothness from the threshold to the final high LET value. In Fig. 4 we report the cross-sections for SEU, SEL and SET as evaluated from our analysis. We estimate SEE threshold of 10.3 ± 1.3 MeV cm^2 mg^{-1} for SEU, 7.6 ± 2.0 MeV cm^2 mg^{-1} for SEL, and 9.2 ± 1.95 MeV cm^2 mg^{-1} for SET. The final cross-sections are $(9.97 \pm 2.15) \times 10^{-5}$ cm^2, $(8.40 \pm 0.62) \times 10^{-5}$ cm^2 and $(6.45 \pm 2.62) \times 10^{-5}$ cm^2 for SEU, SEL and SET respectively. Results are presented in Figures 4. For SET analysis, we discard the time in which the system was in Latch-up. Furthermore, we notice that the fast SET acquisition was affected by dead times (probably

[2]*Stopping and Range of Ions in Matter* is a package of computer programs used to calculate interactions between ions and matter. It is available at http://www.srim.org/

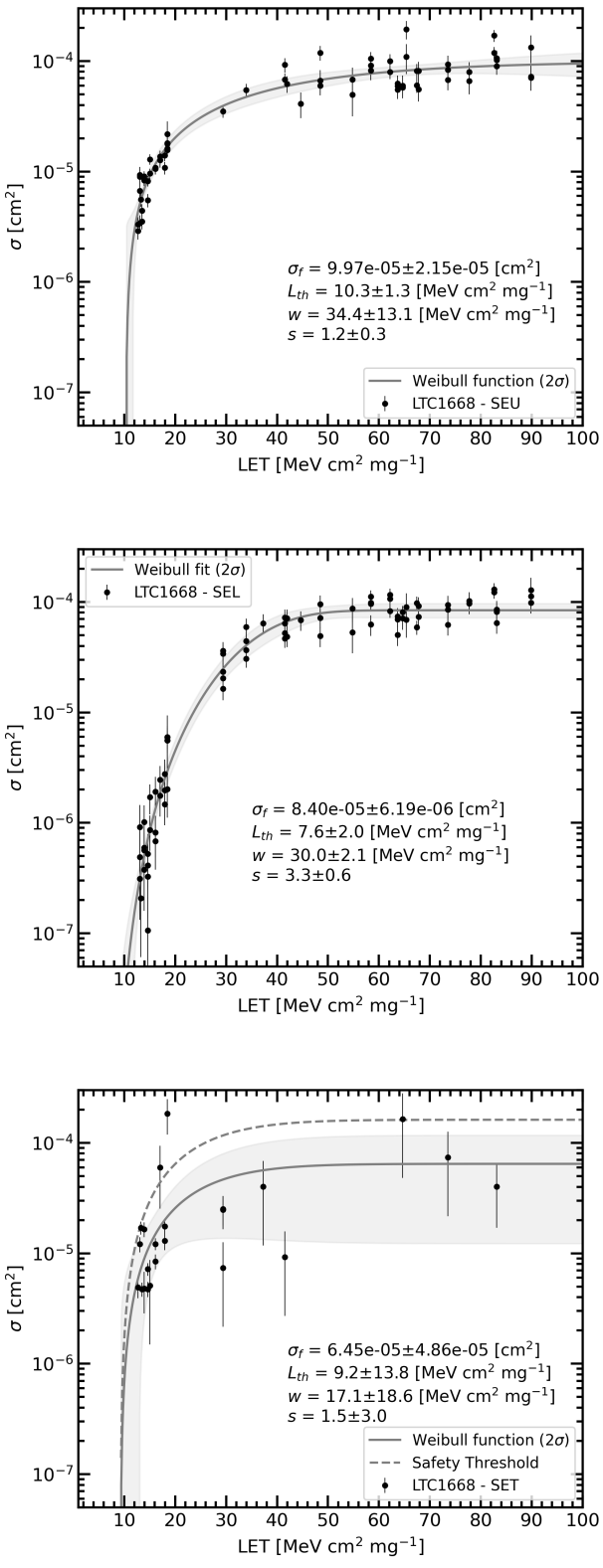

Fig. 4. Computed cross-section for SEU (top), SEL (middle) and SET (bottom) values along with the best fit with the Weibull function in Eq. (3). The shaded area represents 2σ uncertainties from the fit procedure.

associated with data dump from the oscilloscope RAM to the computer storage disk), which occurred unpredictably. The combined effect was a systematic uncertainty that we couldn't properly assess. The runs in which this problem has been identified were excluded from the analysis. Furthermore, for the same reason, we also excluded runs at high LET (i.e., the ones with more SELs) with less than 2 SET occurrences. This also explains why data points are sparser and more scattered in the bottom panel of Figure 4-bottom than the others. Nevertheless, a threshold value of LET, together with the final values of $\sigma(L)$ never exceeding 2×10^{-4} cm^2, can be neatly spotted. The fit proposed in SET analysis was evaluated with an iterative procedure where, at first, all parameters of the Weibull function were free; then we fixed w and s parameters while performing again the fit and exploring the 2σ band. In the same figure, we define as the *safety threshold* the result of the Weibull fit, considering σ_f and L_{th} values in the worst 2σ case.

B. SEE rate

The SEE cross-sections obtained in this work are used to estimate the number of SEE events per device that could be statistically experienced during the on-orbit operations due to direct ionization of heavy nuclei galactic cosmic rays. The Direct-Ionization-Induced SEE was evaluated according to the ECSS guidelines [8] using the CRÈME software [13].

Results of our computation are reported in table IV for three different conditions: i) during a solar minimum, ii) during a solar maximum, and iii) during the worst day. The three cases cover respectively: i) the pessimistic scenario (i.e., the highest galactic cosmic rays flux intensity), ii) the optimistic scenario (i.e., the lowest galactic cosmic rays flux intensity), and, finally, iii) the scenario for 18 hours of exposure at the most intense SEP registered. The CRÈME software includes a set of online tools for SEE rate prediction developed in collaboration with NASA. The computed fluences in the three scenarios are then transported through 100 mils of aluminium to account for the effects due to standard shielding. Finally, the direct-ionization-heavy-ion-induced SEE was evaluated using the HUP module, which calculates direct-ionization rates using the integral rectangular parallelepiped (IRPP) method. Assuming 9 years of operations in space and no. In the case of a continuous high galactic cosmic rays flux, it is expected that in 9 years, on average, about one LTC1668 device, every 2 installed will suffer at least one SEE event (including SEU, SEL and SET) due to direct ionization of heavy nuclei galactic cosmic rays.

IV. Conclusions

We tested the 16-bit DAC LTC1668 from Linear Technology at room temperature under a beam of different ions spanning a LET range from 12 to 90 MeV cm^{-2}mg^{-1}. The irradiation test on LTC1668 using heavy ions shows that the device is moderately sensitive to SEE, with a threshold LET of 10.3 ± 1.3 MeV cm^2 mg^{-1} for SEU, 7.6 ± 2.0 MeV cm^2 mg^{-1} for SEL, and 9.2 ± 1.95 MeV cm^2 mg^{-1} for SET. The saturation (final) cross-section values are $(9.97 \pm 2.15) \times 10^{-5}$ cm^2, $(8.40 \pm 0.62) \times 10^{-5}$ cm^2 and $(6.45 \pm 2.62) \times 10^{-5}$

TABLE IV
NUMBER OF SEE/DEVICE/DAY IN CASE OF A PARALLELEPIPED WITH X = 2.00 MM, Y = 2.95 MM, AND Z = 1 μM. IN THE SET COLUMN, WE REPORT IN PARENTHESES THE VALUE USING THE SAFETY THRESHOLD CROSS-SECTION. FOR THE SEP WORST DAY, THE NUMBER OF SEE IS EVALUATED FOR AN EXPOSITION OF 18 HOURS.

	SEL	SEU	SET (safety threshold)
Solar minimum [SEE/device/day]	5.37×10^{-5}	8.41×10^{-5}	5.28×10^{-5} (2.83×10^{-4})
Solar Maximum [SEE/device/day]	1.92×10^{-5}	3.04×10^{-5}	3.36×10^{-5} (1.05×10^{-4})
SEP WORST-DAY [SEEs/device in 18 hours]	4.02×10^{-1}	6.49×10^{-1}	7.25×10^{-1} (2.33)

cm^2 for SEU, SEL and SET respectively. SEL cannot be considered as a rare event, therefore a suitable SEL circumvention circuitry should be implemented. A significant number of SEUs is observed, which induces the wrong output value. The output should be reset after reprogramming the DAC registers. Numerous SETs were observed with different time characteristics and populations. They show up as a blend of short ($< 1\mu s$) and long ($> 1\mu s$) pulses. Overall, the cross-section of transient events exhibits a threshold around 10 MeV cm^2 mg^{-1}, reaching rapidly a saturation value $\leq 2 \times 10^{-4}$ cm^2. Considering the SEE rate evaluated for the computed cross-sections, we conclude that the DAC LTC1664 could be considered for space application, assessing a proper radiation shielding and automatic recovery procedure to minimize the (already low) risk of SEE-induced damage. Further study (e.g., SEL tests at higher temperatures) are required to be space-qualified. [14]

ACKNOWLEDGMENT

We would acknowledge M. Tacconi of University of Milano-Bicocca for the useful discussion and address on the use of SR-Niel calculator. We thank the LNL staff, in particular the operators of the Tandem accelerator. We acknowledge the financial support of INFN and the Italian Space Agency (ASI) through the LITEBIRD program, and the ASI Grants n. 2016–24-H.1-2018 and 2020-9-HH.0

REFERENCES

[1] E. Allys *et al.*, "Probing cosmic inflation with the litebird cosmic microwave background polarization survey," 2022.

[2] M. Kamionkowski and E. D. Kovetz, "The quest for b modes from inflationary gravitational waves," *Annual Review of Astronomy and Astrophysics*, vol. 54, no. 1, pp. 227–269, 2016. [Online]. Available: https://doi.org/10.1146/annurev-astro-081915-023433

[3] R. W. Besuner, "Design, planning, and performance of the CMB-S4 experiment," in *Ground-based and Airborne Telescopes IX*, H. K. Marshall, J. Spyromilio, and T. Usuda, Eds., vol. 12182, International Society for Optics and Photonics. SPIE, 2022, p. 121821D. [Online]. Available: https://doi.org/10.1117/12.2636149

[4] Tauber, J. A., Mandolesi, N., Puget, J.-L. *et al.*, "Planck pre-launch status: The planck mission," *A&A*, vol. 520, p. A1, 2010. [Online]. Available: https://doi.org/10.1051/0004-6361/200912983

[5] M. Durante and F. A. Cucinotta, "Heavy ion carcinogenesis and human space exploration," *Nature Reviews Cancer*, vol. 8, no. 6, pp. 465–472, Jun. 2008.

[6] S. W. Samwel and A. A. Hady, "Space radiation environment forecast for egyptsat-2 satellite," *Space Weather*, vol. 7, no. 12, p. S12004, 2009.

[7] Y. Gonzalez-Velo, H. J. Barnaby, and M. N. Kozicki, "Review of radiation effects on ReRAM devices and technology," *Semiconductor Science Technology*, vol. 32, no. 8, p. 083002, Aug. 2017.

[8] ECSS, *ECSS-E-HB-10-12A Space engineering - Calculation of radiation and its effects and margin policy handbook*, ESA-ESTEC, Requirements and Standards Division, Noordwijk, The Netherlands, 2010.

[9] E. Petersen, *Single Event Effects in Aerospace*. 445 Hoes Lane, Piscataway, NJ 08854: Wiley-IEEE Press, 2011. [Online]. Available: https://ieeexplore.ieee.org/servlet/opac?bknumber=6047596

[10] L. Silvestrin, D. Bisello, A. Candelori, P. Giubilato, S. Mattiazzo, D. Pantano, M. Tessaro, and J. Wyss, "Status and prospects of the sirad irradiation facility for radiation effects studies at lnl," in *2013 14th European Conference on Radiation and Its Effects on Components and Systems (RADECS)*, 2013, pp. 1–4.

[11] M. Boschini, P. Rancoita, and M. Tacconi, "Sr-niel calculator: Screened relativistic (sr) treatment for calculating the displacement damage and nuclear stopping powers for electrons, protons, light- and heavy- ions in materials (version 7.7.3)," http://www.sr-niel.org/, 2014, available at INFN sez. Milano-Bicocca, Italy. Accessed: Feb. 2021.

[12] ESCC, *Single Event Effects Test Method and guidelines - ESCC Basic Specification No. 25100*, ESA, Requirements and Standards Division, Noordwijk, The Netherlands, 2014.

[13] A. Tylka, J. Adams, P. Boberg, B. Brownstein, W. Dietrich, E. Flueckiger, E. Petersen, M. Shea, D. Smart, and E. Smith, "Creme96: A revision of the cosmic ray effects on micro-electronics code," *IEEE Transactions on Nuclear Science*, vol. 44, no. 6, pp. 2150–2160, 1997.

[14] S. Zhang, C. Zhu, J. K. O. Sin, and P. K. T. Mok, "A novel ultrathin elevated channel low-temperature poly-Si TFT," *IEEE Electron Device Lett.*, vol. 20, pp. 569–571, Nov. 1999.

TABLE V

LOG TABLE OF IRRADIATION CAMPAIGNS ALONG WITH THE NUMBER OF SEU AND SEL DETECTION AND CROSS-SECTION.

date	Run id	Sample	Ion	[a] [deg]	Eff. LET [b]	Irr. time [s]	Eff. Fluence [cm^{-2}]	SEL n. Ev.	SEL σ [cm^2]	SEU n. Ev.	SEU σ [cm^2]	Test conditions
2021	117	DUT1	I-127	0	65.37	0:10:53	1.01E+05	9	8.96E-05	11	1.09E-04	
2021	118	DUT0	I-127	0	65.37	0:14:18	1.44E+05	10	6.93E-05	28	1.94E-04	
2021	119	DUT0	Cl-35	0	12.68	0:13:07	1.20E+07	0	0.00E+00	40	3.32E-06	
2021	131	DUT0	Cl-35	30	14.64	0:16:14	9.47E+06	1	1.06E-07	52	5.49E-06	
2021	132	DUT0	Cl-35	20	13.49	0:13:37	1.19E+07	0	0.00E+00	42	3.53E-06	
2021	133	DUT0	Cl-35	45	17.93	0:16:17	5.44E+06	8	1.47E-06	76	1.40E-05	
2021	134	DUT0	Cl-35	38	16.09	0:17:17	7.33E+06	5	6.82E-07	78	1.06E-05	
2021	135	DUT1	Cl-35	0	12.68	0:18:11	1.21E+07	0	0.00E+00	35	2.90E-06	
2021	136	DUT1	Cl-35	20	13.49	0:14:54	1.13E+07	0	0.00E+00	50	4.42E-06	
2021	137	DUT1	Cl-35	30	14.64	0:16:05	9.74E+06	4	4.11E-07	80	8.21E-06	
2021	138	DUT1	Cl-35	38	16.09	0:14:44	7.31E+06	6	8.20E-07	79	1.08E-05	
2021	139	DUT1	Cl-35	45	17.93	0:19:28	5.55E+06	11	1.98E-06	60	1.08E-05	
2021	140	DUT2	Cl-35	45	17.93	0:10:46	2.90E+06	8	2.76E-06	44	1.52E-05	
2021	141	DUT2	Cl-35	38	16.09	0:10:38	4.18E+06	8	1.92E-06	35	8.38E-06	
2021	142	DUT2	Cl-35	30	14.64	0:10:01	9.19E+06	3	3.26E-07	58	6.31E-06	
2021	143	DUT2	Cl-35	30	14.64	0:09:05	7.62E+06	4	5.25E-07	66	8.66E-06	
2021	148	DUT0	Ni-58	0	29.36	0:27:14	1.34E+06	22	1.64E-05	23	1.71E-05	
2021	175	DUT0	Ni-58	0	29.36	0:34:08	7.46E+05	27	3.62E-05	-	-	[c]
2021	180	DUT0	Ni-58	45	41.52	0:34:54	4.16E+05	30	7.22E-05	-	-	[c]
2021	181	DUT1	Ni-58	45	41.52	0:38:32	6.85E+05	32	4.67E-05	40	5.84E-05	
2021	183	DUT1	Ni-58	30	33.90	0:31:02	5.86E+05	26	4.44E-05	27	4.61E-05	
2021	184	DUT0	Ni-58	30	33.90	0:34:01	6.82E+05	25	3.66E-05	-	-	[c]
2021	185	DUT1	Ni-58	0	29.36	0:32:56	1.11E+06	26	2.34E-05	30	2.70E-05	
2021	186	DUT1	Ni-58	0	29.36	0:20:08	1.77E+06	36	2.04E-05	62	3.51E-05	
2021	187	DUT1	Ni-58	30	33.90	0:17:23	1.08E+06	33	3.07E-05	59	5.48E-05	
2021	188	DUT1	Ni-58	45	41.52	0:20:15	7.36E+05	47	6.39E-05	50	6.79E-05	
2021	189	DUT0	Ni-58	0	29.36	0:14:52	7.37E+05	25	3.39E-05	18	2.44E-05	[c]
2021	191	DUT0	Ni-58	30	33.90	0:09:54	4.55E+05	27	5.93E-05	-	-	[c]
2021	192	DUT0	Ni-58	45	41.52	0:09:34	4.77E+05	25	5.24E-05	44	9.23E-05	
2021	193	DUT0	Ni-58	38	37.26	0:10:48	3.75E+05	24	6.40E-05	-	-	[c]
2021	208	DUT0	Ag-10	0	58.39	0:18:00	5.02E+05	56	1.12E-04	-	-	[c]
2021	209	DUT1	Ag-10	0	58.39	0:08:59	3.52E+05	22	6.25E-05	29	8.24E-05	
2021	210	DUT1	Ag-10	0	58.39	0:16:57	5.62E+05	54	9.61E-05	46	1.05E-04	
2021	211	DUT1	Ag-10	20	62.14	0:17:17	6.26E+05	52	8.30E-05	50	7.98E-05	
2021	212	DUT1	Ag-10	30	67.42	0:17:06	7.99E+05	47	5.88E-05	48	6.01E-05	
2021	213	DUT1	Ag-10	45	82.58	0:23:22	5.40E+05	66	1.22E-04	64	1.19E-04	
2021	214	DUT0	Ag-10	20	62.14	0:14:06	3.75E+05	40	1.07E-04	-	-	[c]
2021	215	DUT2	Ag-10	0	58.39	0:14:22	4.59E+05	45	9.81E-05	42	9.16E-05	
2021	216	DUT2	Ag-10	20	62.14	0:15:48	4.39E+05	51	1.16E-04	44	1.00E-04	
2021	217	DUT2	Ag-10	30	67.42	0:16:37	4.91E+05	48	9.77E-05	40	8.14E-05	
2021	218	DUT2	Ag-10	45	82.58	0:17:36	4.00E+05	52	1.30E-04	68	1.70E-04	
2022	1	DUT1	Cl-35	0	13.05	0:47:02	9.61E+06	3	3.12E-07	64.5	6.71E-06	
2022	2	DUT1	Cl-35	10	13.25	0:55:36	9.60E+06	2	2.08E-07	53.5	5.57E-06	
2022	3	DUT1	Cl-35	20	13.89	0:54:35	8.87E+06	5	5.64E-07	74	8.35E-06	
2022	4	DUT1	Cl-35	20	13.89	0:35:18	5.88E+06	6	1.02E-06	0	0.00E+00	
2022	5	DUT1	Cl-35	30	15.07	0:57:42	9.31E+06	8	8.59E-07	89.5	9.61E-06	
2022	6	DUT1	Cl-35	40	17.04	0:42:46	3.66E+06	9	2.46E-06	46.5	1.27E-05	
2022	7	DUT1	Cl-35	45	18.46	0:06:22	5.04E+05	3	5.95E-06	11	2.18E-05	
2022	8	DUT1	Cl-35	45	18.46	0:21:16	1.43E+06	8	5.58E-06	25.5	1.78E-05	
2022	9	DUT2	Cl-35	0	13.05	0:10:50	3.27E+06	3	9.18E-07	30.5	9.34E-06	
2022	10	DUT3	Cl-35	0	13.05	0:13:00	1.01E+07	-	-	34.5	3.43E-06	
2022	11	DUT3	Cl-35	20	13.89	0:11:57	7.96E+06	3	3.77E-07	69	8.67E-06	
2022	12	DUT3	Cl-35	40	17.04	0:12:06	4.55E+06	8	1.76E-06	62.5	1.37E-05	
2022	13	DUT3	Cl-35	45	18.46	0:09:26	2.47E+06	5	2.02E-06	40	1.62E-05	
2022	14	DUT3	Cl-35	45	18.46	0:25:50	3.53E+06	21	5.96E-06	55.5	1.57E-05	
2022	15	DUT2	Cl-35	45	18.46	0:25:02	3.59E+06	20	5.58E-06	65	1.81E-05	
2022	16	DUT2	Cl-35	30	15.07	0:26:12	6.42E+06	11	1.71E-06	82.5	1.29E-05	
2022	17	DUT2	Cl-35	20	13.89	0:28:25	8.38E+06	5	5.97E-07	75.5	9.01E-06	
2022	18	DUT2	Cl-35	0	13.05	0:15:23	4.08E+06	2	4.90E-07	36.5	8.94E-06	
2022	19	DUT1	I-127	0	63.66	0:28:21	5.73E+05	40	6.98E-05	31.5	5.50E-05	
2022	20	DUT1	I-127	10	64.64	0:37:43	6.57E+05	53	8.07E-05	38	5.78E-05	
2022	21	DUT1	I-127	10	64.64	0:30:53	3.09E+05	22	7.12E-05	18.5	5.99E-05	

continue in Table VI...

[a] Incidence Angle of the Flux [MeV cm^2/mg]

[b] Effective LET in Si [MeV cm^2/mg]

[c] DUT0 damaged, not relaiable for SEU

TABLE VI

LOG TABLE OF IRRADIATION CAMPAIGNS ALONG WITH THE NUMBER OF SEU AND SEL DETECTION AND CROSS-SECTION.

date	Run id	Sample	Ion	[a] [deg]	Eff. LET [b]	Irr. time [s]	Eff. Fluence [cm^{-2}]	SEL n. Ev.	SEL σ [cm^2]	SEU n. Ev.	SEU σ [cm^2]	Test conditions
continue from Table V												
2022	22	DUT1	I-127	30	73.51	0:38:37	3.86E+05	24	6.22E-05	26	6.74E-05	
2022	23	DUT1	I-127	45	89.87	0:14:45	9.40E+04	12	1.28E-04	12.5	1.33E-04	
2022	24	DUT1	I-127	40	83.10	0:30:15	3.07E+05	25	8.16E-05	32.5	1.06E-04	
2022	25	DUT1	I-127	35	77.71	0:25:19	2.45E+05	25	1.02E-04	19.5	7.97E-05	
2022	26	DUT2	I-127	0	63.66	0:20:33	4.57E+05	23	5.04E-05	28.5	6.24E-05	
2022	27	DUT2	I-127	20	67.75	0:11:42	2.82E+05	26	9.21E-05	23	8.15E-05	
2022	28	DUT2	I-127	30	73.51	0:21:03	2.69E+05	23	8.55E-05	25	9.30E-05	
2022	29	DUT2	I-127	40	83.10	0:22:43	3.04E+05	26	8.55E-05	31	1.02E-04	
2022	30	DUT2	I-127	45	89.87	0:19:35	2.21E+05	25	1.13E-04	16	7.23E-05	
2022	31	DUT2	I-127	35	77.71	0:20:29	2.58E+05	25	9.70E-05	17	6.60E-05	
2022	32	DUT3	I-127	0	63.66	0:22:43	3.79E+05	28	7.39E-05	22.5	5.94E-05	
2022	33	DUT3	I-127	30	73.51	0:19:11	2.65E+05	25	9.44E-05	22	8.31E-05	
2022	34	DUT3	I-127	20	67.75	0:21:03	3.42E+05	25	7.32E-05	19	5.56E-05	
2022	35	DUT3	I-127	45	89.87	0:20:54	2.54E+05	25	9.83E-05	18	7.07E-05	
2022	36	DUT3	I-127	40	83.10	0:26:54	3.88E+05	25	6.44E-05	35	9.01E-05	
2022	37	DUT1	Br-79	0	41.96	0:22:20	5.38E+05	26	4.83E-05	33.5	6.22E-05	
2022	39	DUT1	Br-79	20	44.65	0:17:16	3.65E+05	25	6.84E-05	15	4.11E-05	
2022	40	DUT1	Br-79	30	48.45	0:14:18	2.63E+05	25	9.52E-05	17.5	6.66E-05	
2022	41	DUT1	Br-79	40	54.77	0:13:09	1.84E+05	16	8.71E-05	12.5	6.81E-05	
2022	42	DUT2	Br-79	30	48.45	0:53:02	3.48E+05	25	7.18E-05	41.5	1.19E-04	
2022	43	DUT3	Br-79	30	48.45	0:35:19	4.67E+05	23	4.93E-05	28	6.00E-05	
2022	44	DUT3	Br-79	40	54.77	0:15:29	1.51E+05	8	5.29E-05	7.5	4.96E-05	

[a] Incidence Angle of the Flux [MeV cm^2/mg]

[b] Effective LET in Si [MeV cm^2/mg]

TABLE VII

LOG TABLE OF IRRADIATION CAMPAIGNS ALONG WITH THE NUMBER OF SET DETECTION AND CROSS-SECTION.

date	Run id	Sample	Ion	Eff. LET [a]	SET n. Ev.	SET σ [cm^2]
2021	118	DUT0	I-127	65.37	4	1.20E-04
2021	119	DUT0	Cl-35	12.68	24	4.90E-06
2021	131	DUT0	Cl-35	14.64	40	4.70E-06
2021	133	DUT0	Cl-35	17.93	53	1.80E-05
2021	134	DUT0	Cl-35	16.09	67	1.20E-05
2021	136	DUT1	Cl-35	13.49	47	4.70E-06
2021	137	DUT1	Cl-35	14.64	58	7.20E-06
2021	138	DUT1	Cl-35	16.09	44	8.40E-06
2021	139	DUT1	Cl-35	17.93	33	1.30E-05
2021	185	DUT1	Ni-58	29.36	9	2.50E-05
2021	186	DUT1	Ni-58	29.36	12	2.50E-05
2021	187	DUT1	Ni-58	33.90	1	5.20E-06
2021	188	DUT1	Ni-58	41.52	2	9.20E-06
2021	212	DUT1	Ag-107	67.42	1	5.40E-05
2022	1	DUT1	Cl-35	13.05	40	1.20E-05
2022	2	DUT1	Cl-35	13.25	55	1.70E-05
2022	3	DUT1	Cl-35	13.89	43	1.60E-05
2022	5	DUT1	Cl-35	15.07	54	1.90E-05
2022	6	DUT1	Cl-35	17.04	71	8.40E-05
2022	7	DUT1	Cl-35	18.46	8	1.80E-04
2022	16	DUT2	Cl-35	15.07	2	5.10E-06
2022	17	DUT2	Cl-35	13.89	6	4.80E-06
2022	21	DUT1	I-127	64.64	2	1.60E-04
2022	22	DUT1	I-127	73.51	2	7.40E-05
2022	24	DUT1	I-127	83.10	3	4.00E-05
2022	25	DUT1	I-127	77.71	4	8.00E-05
2022	37	DUT1	Br-79	41.96	13	1.50E-04
2022	41	DUT1	Br-79	54.77	1	4.80E-04

[a] Effective LET in Si [MeV cm^2/mg]